J Adv Ceram

Rapid Communication

Mn-α-SiAlON: A new member of α-SiAlON family

Shijia Zhang[1], Dengke Zhao[1], Kexin Chen[2,✉], Guanghua Liu[1,✉]

Cite this article: Zhang S, Zhao D, Chen K, et al. *J Adv Ceram* 2026, **15**(3): 9221249. https://doi.org/10.26599/JAC.2026.9221249

ABSTRACT: α-SiAlON, as a solid solution of α-Si_3N_4, is a valuable ceramic material due to its excellent mechanical and functional properties. The structure of α-SiAlON is necessarily stabilized by so-called stabilizing cations. To date, various stabilizing cations, including Li, Mg, Ca, Sr, and most rare earth elements, have been used in α-SiAlON, but no α-SiAlON stabilized with transition metal cations has been reported. In this work, we report Mn-α-SiAlON as a new member of the α-SiAlON family and, to the best of our knowledge, the first example of α-SiAlON stabilized with transition metal cations. Single-phase Mn-α-SiAlON with a nominal chemical composition of $Mn_{0.75}Si_{9.75}Al_{2.25}O_{0.75}N_{15.25}$ was prepared by spark plasma sintering from a precursor powder mixture of α-Si_3N_4, AlN, and MnO. The formation of Mn-α-SiAlON isostructural to α-Si_3N_4 was confirmed by X-ray diffraction (XRD) and transmission electron microscopy (TEM). The new Mn-α-SiAlON exhibited a superior Vickers hardness of 23.1 GPa, good fracture toughness of 6.7 MPa·$m^{1/2}$, and thermal conductivity of 7.60 W/(m·K). We hope that the discovery of Mn-α-SiAlON will open new possibilities for tailoring the chemical composition and optimizing the properties of α-SiAlON.

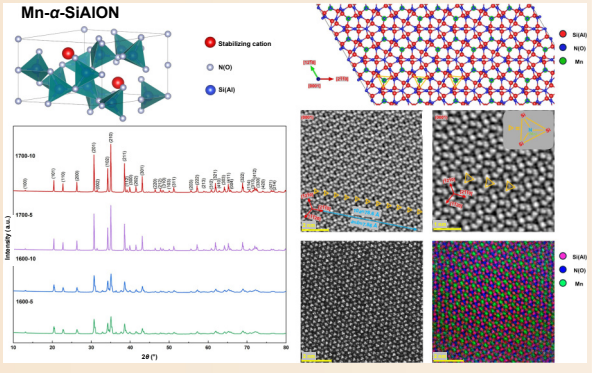

KEYWORDS: α-SiAlON; stabilizing cation; Mn-α-SiAlON

1 Introduction

α-SiAlON is the solid solution of α-Si_3N_4 formed by partially substituting Si by Al and N by O without changing the lattice structure [1–4]. α-SiAlON is recognized as an important ceramic material due to its unique mechanical [5–13], thermal [14–17], and optical properties [18–24]. In α-SiAlON, Si–N bonds are partially replaced with Al-O and Al-N bonds, and so-called stabilizing cations are incorporated into interstitial sites for charge balance, as shown in Fig. 1. The chemical formula of α-SiAlON is $M_xSi_{12-m-n}Al_{m+n}O_nN_{16-n}$ ($m > 0$; $n > 0$; $x = m/v$, v is the valence of the stabilizing cation M) [1], where $0 < x \leq 2$ because each unit cell of α-SiAlON contains only two interstitial sites [3]. The kind of stabilizing cations has a strong influence on the structural stability and properties of α-SiAlON. For example, it was reported that the kind of stabilizing cations affected the grain morphology of α-SiAlON, and proper choice of stabilizing cations promoted the growth of rod-like grains, which enabled high toughness and hardness [5,25–30]. Moreover, the stabilizing cations were revealed to have a significant influence on the thermal properties of α-SiAlON [14–16,31–33].

Since the discovery of α-SiAlON in the 1970s, various stabilizing cations that can fully stabilize the α-SiAlON structure have been reported, including Li, Mg, Ca, Sr, and most rare earth elements [3,34–36]. Nevertheless, to the best of our knowledge, no α-SiAlON stabilized with transition metal cations has been reported yet. Recently, we explored the possibility of nearly twenty kinds of transition metal cations (e.g., Ti, Cr, Fe, Co, Ni, and Cu) in stabilizing α-SiAlON. However, most of the cations failed to stabilize the α-SiAlON structure, and single-phase α-SiAlON was obtained only for Mn^{2+}.

In this work, we report Mn-α-SiAlON as a new member of the α-SiAlON family and the first example of α-SiAlON stabilized with transition metal cations. Single-phase Mn-α-SiAlON with a nominal chemical composition of $Mn_{0.75}Si_{9.75}Al_{2.25}O_{0.75}N_{15.25}$ was prepared by spark plasma sintering from a precursor powder mixture of α-Si_3N_4, AlN, and MnO. The crystal structure and mechanical and thermal properties of Mn-α-SiAlON were investigated.

2 Experimental

Commercial powders of α-Si_3N_4 (UBE-E10), AlN, and MnO were used as raw materials. The powders were weighed and mixed according to the nominal composition of $Mn_{0.75}Si_{9.75}Al_{2.25}O_{0.75}N_{15.25}$ (m = 1.5, n = 0.75), homogenized by ball-milling with ethanol and dried in an oven at 60 °C for 12 h. Next, the powder mixture was poured into a graphite mold and densified by spark

[1]State Key Laboratory of New Ceramic Materials, School of Materials Science and Engineering, Tsinghua University, Beijing 100084, China. [2]State Key Laboratory for Advanced Metals and Materials, University of Science and Technology Beijing, Beijing 100083, China.

✉ Corresponding authors. E-mail: K. Chen, kxchen@ustb.edu.cn; G. Liu, liuguanghua@mail.tsinghua.edu.cn

Received: November 23, 2025; Revised: December 26, 2025; Accepted: January 11, 2026

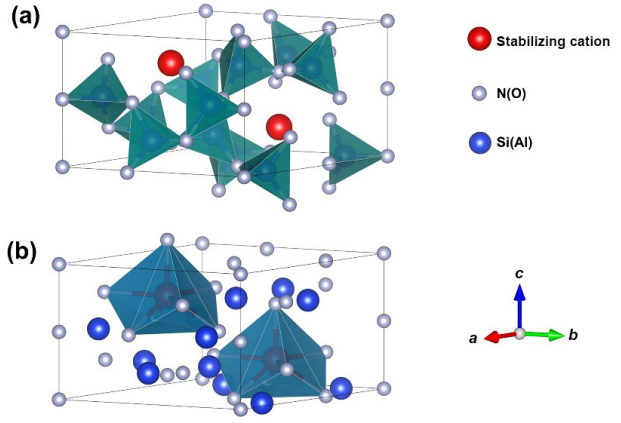

Fig. 1 Unit cell of α-SiAlON: (a) marking Si–N(4) polyhedrons; (b) marking M–N(7) polyhedrons.

plasma sintering (SPS) at 1600/1700 °C for 5/10 min under a mechanical pressure of 100 MPa to produce Mn-α-SiAlON samples of different sintering procedures. The samples were named after their sintering procedures, and for example, "1600-5" referred to the sample fabricated by SPS at 1600 °C for 5 min.

The phase composition of polished bulk samples was characterized by X-ray diffraction (XRD) using Cu-Kα at a scanning rate of 1 (°)/min, and the lattice parameters were obtained by lattice refinement using the GSAS-II software [37]. The microstructure and crystal structure were examined by scanning electron microscopy (SEM), transmission electron microscopy (TEM), and scanning transmission electron microscopy (STEM). TEM samples were prepared by focused ion beam (FIB). Elemental analysis was performed by energy dispersive spectroscopy (EDS) and electron energy loss spectroscopy (EELS).

The bulk density of the samples was determined by the Archimedes method. Vickers hardness and fracture toughness were measured by the indentation method on a polished sample surface with a load of 9.8 N. Thermal diffusivity/conductivity was tested by the laser flash method (LFA-467, Netzsch).

3 Results and discussion

The XRD patterns of the sintered samples are shown in Fig. 2(a). It is evident that single-phase α-SiAlON was obtained in the samples sintered at 1700 °C. For the samples sintered at a lower temperature of 1600 °C, the XRD patterns also correspond to the α-SiAlON phase, but the peak intensity is lower, and peak widening or splitting occurs due to the presence of unreacted α-Si_3N_4. In general, the synthesis of α-SiAlON is realized by the dissolution-precipitation mechanism in a coexisting liquid phase, where α-Si_3N_4 particles are dissolved and α-SiAlON crystallites are precipitated [3,4]. The sintering temperature has a strong influence on the volume fraction, the viscosity of the liquid phase and the kinetics of the dissolution-precipitation process. Compared to the samples sintered at 1700 °C, the samples sintered at a lower temperature of 1600 °C had slower reaction kinetics, and the conversion from α-Si_3N_4 to α-SiAlON was incomplete.

Based on the XRD results, the lattice parameters of Mn-α-SiAlON for the 1700-10 and 1700-5 samples were obtained by lattice refinement, as shown in Fig. 2(b) and Table 1. During the refinement, a minimal *wR* (weighted residual factor) of 11.9% was reached. Despite the intensity difference between the calculated and observed XRD peaks, which may be affected by the preferred orientation of α-SiAlON crystallites in the SPS samples, the calculated peak positions agree well with the observed positions. As Table 1 shows, Mn-α-SiAlON exhibits the same lattice structure as α-Si_3N_4 but slightly larger lattice parameters than α-Si_3N_4 ($a = b = 7.75$ Å; $c = 5.62$ Å). Moreover, the experimental results of lattice parameters (1700-10) were compared with the data calculated from empirical formulas in the literature, as shown in Table 2. It is clear that the experimental results agree well with the calculated data from the empirical formulas with deviations no more than 0.5%. This agreement confirms that the Mn-α-SiAlON prepared in this work has a structure similar to that of traditional α-SiAlON members.

The microstructure of the Mn-α-SiAlON samples is examined

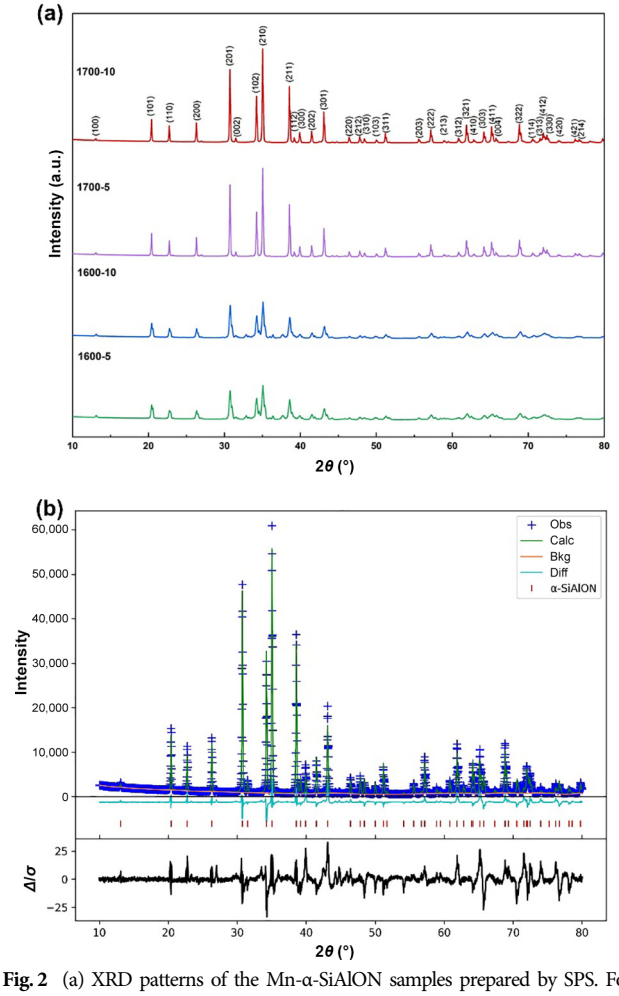

Fig. 2 (a) XRD patterns of the Mn-α-SiAlON samples prepared by SPS. For example, "1700-10" refers to the sample sintered at 1700 °C for 10 min. (b) Refinement plot of the 1700-10 sample (Obs: observed results; Calc: calculated results; Bkg: background; Diff: the difference between observed and calculated results; Δ/σ: relative deviation).

Table 1 Experimental lattice parameters of Mn-α-SiAlON by lattice refinement

Sample	*a* (Å)	*b* (Å)	*c* (Å)	*α* (°)	*β* (°)	*γ* (°)	Cell volume (Å^3)	Theoretical density (g/cm^3)
1700-10	7.8212	7.8212	5.6783	90	90	120	300.812	3.321
1700-5	7.8210	7.8210	5.6785	90	90	120	300.805	3.321

by SEM and TEM, as shown in Figs. 3(a)–3(c). The samples show equiaxed grains, and the grain size increases from several hundred nanometers to more than one micrometer with increasing sintering temperature from 1600 to 1700 °C. The corresponding EDS mapping of Mn in Fig. 3(d) reveals that the distribution of Mn is generally homogeneous on a larger scale despite the segregation of Mn at grain boundaries on a smaller scale. The segregation of Mn may cause a deviation of the actual composition of the Mn-α-SiAlON phase from the nominal composition. This deviation, however, seems insignificant because the experimentally derived lattice parameters of the Mn-α-SiAlON phase agree well with those calculated based on the nominal composition in Table 2. Moreover, the electron diffraction pattern in Fig. 3(e) confirmed that the lattice structure of Mn-α-SiAlON agrees well with the traditional α-SiAlON structure. The high-resolution TEM image in Fig. 3(f) is consistent with the electron diffraction pattern, clearly showing two perpendicular lattice planes with interplanar spacings of 6.77 and 5.68 Å, corresponding to the (100) and (001) planes of α-SiAlON.

The lattice structure of Mn-α-SiAlON at atomic scale is further characterized by comparison with the theoretical structure. The theoretical cell structure of α-SiAlON viewed from the [0001] direction is shown in Fig. 4(a), from which triangles formed by N–Si(3) can be seen with N atoms overlapped by interstitial metal atoms. These triangles were successfully observed in integrated differential phase contrast (IDPC) STEM images, as shown in Figs. 4(b) and 4(c), which were captured along the [0001] direction. The lattice parameter of a ($a = b$) was measured to be 7.86 Å, slightly expanded compared to that of α-Si_3N_4 (a = 7.75 Å). Additionally, the high angular dark field (HAADF) STEM image and EDS shown in Figs. 4(e) and 4(f) verified that Mn was orderly incorporated into the interstitial sites of α-SiAlON, in alignment with the theoretical structure in Fig. 4(a). These atomic-scale characterizations, in addition to the XRD results at the macroscale, further confirm the formation of Mn-α-SiAlON as a new member of the α-SiAlON family.

The valence state of Mn in Mn-α-SiAlON is examined by EELS, as shown in Fig. 4(d). In general, the valence state of Mn can be estimated based on the branching energy difference (ΔE) between the L_2 and L_3 white lines ($\Delta E(L_2 - L_3)$) or the integrated intensity ratio of L_3/L_2. When $\Delta E(L_2 - L_3)$ is larger than 11.4 eV or L_3/L_2 is larger than 3, it can be inferred that Mn is divalent [40,41], i.e., Mn^{2+}. In Fig. 4(d), the branching energy difference for Mn was 11.4 eV, indicating that Mn cations most likely existed in the form of Mn^{2+} in Mn-α-SiAlON. Another piece of evidence is that in Mn-α-SiAlON, the intensity ratio of L_3/L_2 of Mn is 3.4, which also indicates the existence of divalent Mn cations [40,41].

The basic properties, including density, hardness, fracture toughness, and thermal conductivity, of Mn-α-SiAlON and traditional α-SiAlONs are given in Table 3. It was found that a higher sintering temperature and longer holding time resulted in higher density and hardness, and the sample 1700-10 showed a

Table 2 Comparison between the calculated and experimental results of the lattice parameters of Mn α-SiAlON ($m = 1.5$, $n = 0.75$)

Empirical formula (Å)	Stabilizing cation	Calculated lattice parameter (Å)	Deviation from experimental result	Ref.
$a = 7.76 + 0.045m + 0.009n$ $c = 5.62 + 0.04m + 0.008n$	M^{v+}	$a = 7.83$ $c = 5.69$	$\Delta a/a = 0.1\%$ $\Delta c/c = 0.2\%$	[1]
$a = 7.706 + 0.0117m + 0.0824r_M^* + 0.0555x$ $c = 5.578 + 0.0259m + 0.0774r_M + 0.0171n$	M^{v+}	$a = 7.84$ $c = 5.70$	$\Delta a/a = 0.3\%$ $\Delta c/c = 0.4\%$	[38]
$a = 7.749 + 0.0673m + 0.0023n$ $c = 5.632 + 0.055m - 0.0054n$	Ca^{2+}	$a = 7.86$ $c = 5.71$	$\Delta a/a = 0.5\%$ $\Delta c/c = 0.5\%$	[39]

Note: r_M^* is the radius of stabilizing cation.

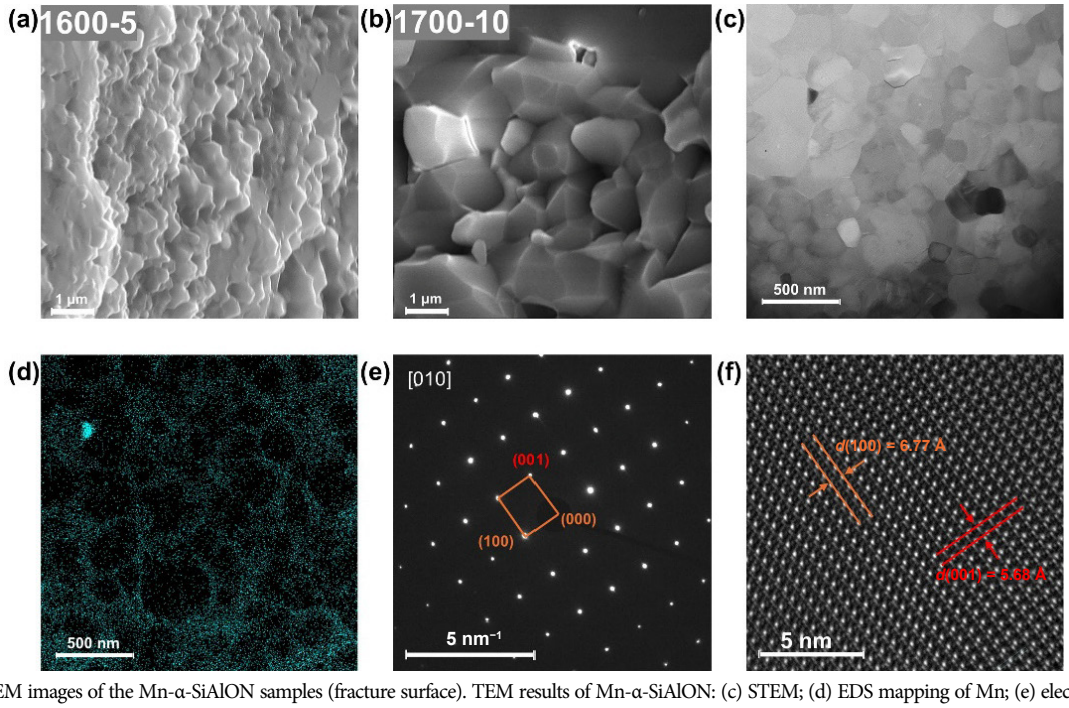

Fig. 3 (a, b) SEM images of the Mn-α-SiAlON samples (fracture surface). TEM results of Mn-α-SiAlON: (c) STEM; (d) EDS mapping of Mn; (e) electron diffraction pattern; (f) high-resolution TEM image.

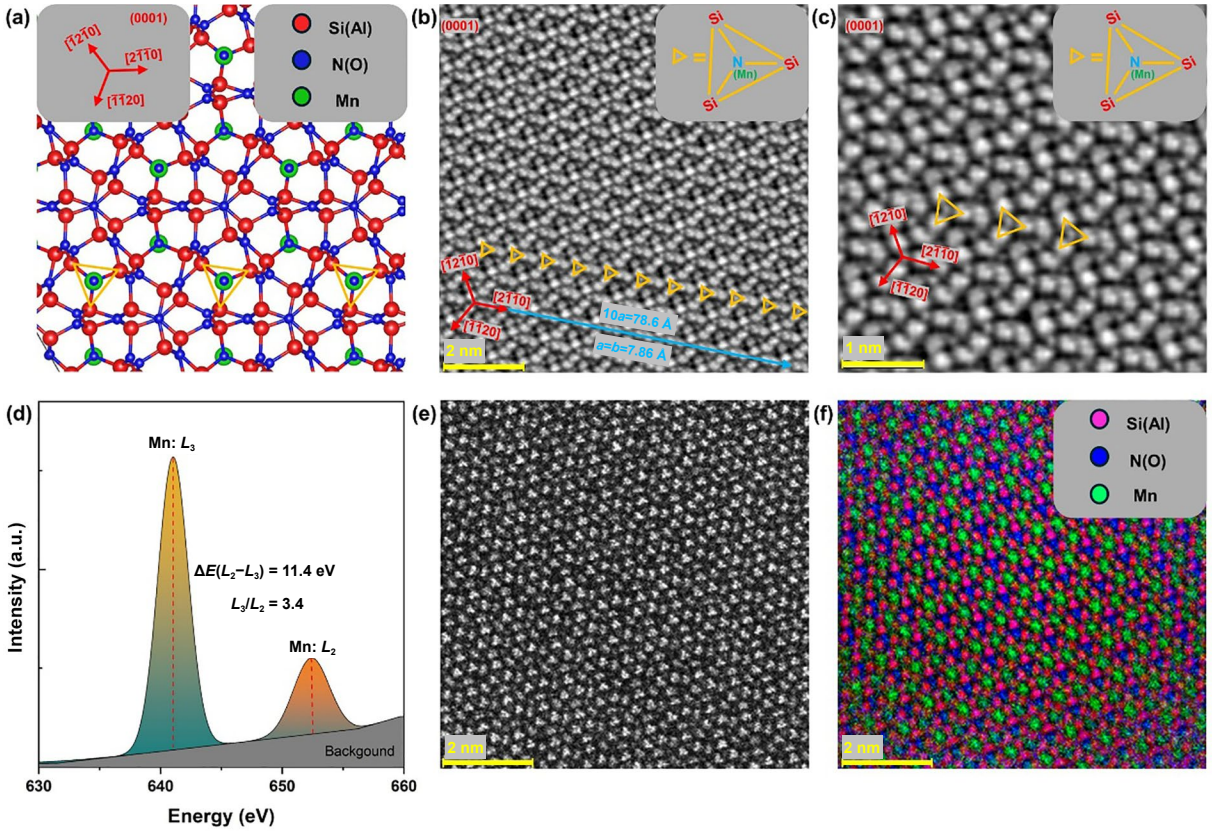

Fig. 4 (a) Theoretical lattice structure of Mn-α-SiAlON. (b, c) IDPC-STEM images of Mn-α-SiAlON. (d) EELS of Mn in Mn-α-SiAlON. (e) HAADF-STEM image of Mn-α-SiAlON; (f) EDS of Mn-α-SiAlON. Triangles formed by N–Si(3) (notated in orange) can be clearly observed along the [0001] direction.

Table 3 Basic properties of Mn-α-SiAlON in this work and traditional α-SiAlONs

Sample	Material	Valence electron of stabilizing element	Bulk density (g/cm^3)	Relative density (%)	Vickers hardness (GPa)	Fracture toughness (MPa·m$^{1/2}$)	Thermal diffusivity (mm^2/s)	Thermal conductivity (W/(m·K))	Ref.
1600-5	Mn-α-SiAlON	$3d^5 4s^2$	3.259	98.1	20.8±0.6	5.0±0.4	3.336	7.25	This work
1600-10	Mn-α-SiAlON	$3d^5 4s^2$	3.267	98.4	21.3±0.9	5.7±0.3	3.343	7.29	This work
1700-5	Mn-α-SiAlON	$3d^5 4s^2$	3.275	98.6	21.7±0.4	5.2±0.4	3.474	7.59	This work
1700-10	Mn-α-SiAlON	$3d^5 4s^2$	3.276	98.6	23.1±0.5	6.7±0.7	3.479	7.60	This work
—	Li-α-SiAlON	2s	3.120	—	20.4±0.1	3.6±0.2	—	—	[46]
—	Mg-α-SiAlON	$3s^2$	—	—	21.4±0.3	6.1±0.1	—	—	[25]
—	Ca-α-SiAlON	$4s^2$	3.170	—	19.8	5.1	—	—	[45]
—	Y-α-SiAlON	$4d5s^2$	—	99.7	17.9	6.4	—	—	[47]
—	Nd-α-SiAlON	$4f^6 6s^2$	—	—	21.7	6.3	—	—	[5]
—	Yb-α-SiAlON	$4f^{14} 6s^2$	—	—	22	5.5	—	—	[6]

Vickers hardness of 23.1 GPa, which is likely the highest record for α-SiAlON materials. At the same time, the fracture toughness of the sample 1700-10 reached 6.7 MPa·m$^{1/2}$, which is also good compared to traditional α-SiAlONs, especially when considering the equiaxed grain morphology (see Figs. 3(a)–3(c)). A clear difference is noticed between the mechanical properties of the 1700-10 and 1700-5 samples, although the two samples are both single-phase α-SiAlON and have similar bulk density. A possible reason is that a longer holding time enables a more complete reaction and results in a higher crystallinity degree of α-SiAlON, as revealed by the XRD results in Fig. 2(a). Moreover, Table 3 shows that Mn is the first reported element with 3d electrons to stabilize α-SiAlON, which provides new opportunities for utilizing α-SiAlON's functional properties, for example, in phosphors. In contrast to the clear difference in mechanical properties, there is no significant difference in the thermal conductivity of the Mn-α-SiAlON samples, which fall in a narrow range of 7.25–7.60 W/(m·K), which is typical for α-SiAlON [42]. By comparison with traditional α-SiAlONs [5,6,9,10,25,42–47], as shown in Fig. 5, the new Mn-α-SiAlON (the sample 1700-10) exhibits superior mechanical properties with a good combination of Vickers hardness and fracture toughness.

4 Conclusions

In this work, Mn-α-SiAlON is developed as a new member of the α-SiAlON family. Single-phase Mn-α-SiAlON bulk samples with a nominal composition of $Mn_{0.75}Si_{9.75}Al_{2.25}O_{0.75}N_{15.25}$ were prepared by spark plasma sintering from a powder mixture of α-Si_3N_4, AlN, and MnO. XRD and TEM characterizations fully confirmed the formation of Mn-α-SiAlON isostructural to α-Si_3N_4 but with an expanded lattice. HAADF-STEM images revealed the orderly

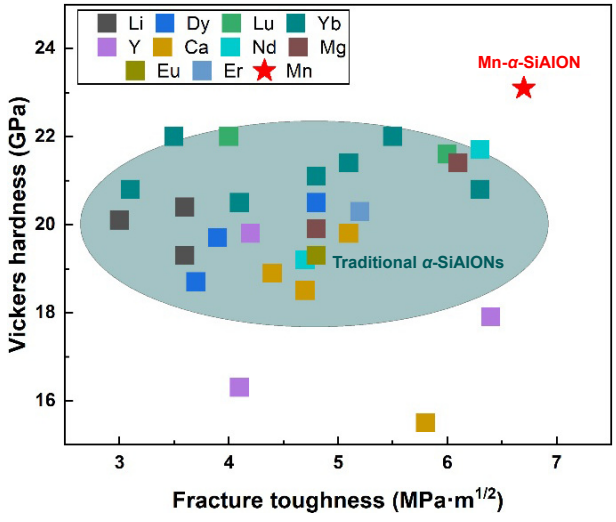

Fig. 5 Comparison between the mechanical properties of Mn-α-SiAlON and those of traditional α-SiAlONs stabilized by Li, Mg, Ca, and rare-earth metals.

distribution of Mn atoms in the lattice of Mn α-SiAlON, and the EELS results suggested that in Mn-α-SiAlON, Mn mostly existed in the divalent state (Mn^{2+}). The new Mn-α-SiAlON showed a superior hardness of 23.1 GPa, good fracture toughness of 6.7 MPa·$m^{1/2}$, and thermal conductivity of 7.60 W/(m·K). To the best of our knowledge, Mn-α-SiAlON is the first example of α-SiAlON stabilized with transition metal cations, and its discovery may open new possibilities for tailoring both the mechanical and functional properties of α-SiAlON.

Acknowledgements

This work is supported by the National Natural Science Foundation of China (Grant No. 52425204).

Availability of data and materials

The data that support the findings of this study are available from the corresponding author upon reasonable request.

Competing interests

The authors have no competing interests to declare that are relevant to the content of this article.

References

[1] Hampshire S, Park HK, Thompson DP, *et al.* α′-sialon ceramics. *Nature* 1978, **274**: 880–882.
[2] Jack KH. Sialons and related nitrogen ceramics. *J Mater Sci* 1976, **11**: 1135–1158.
[3] Cao GZ, Metselaar R.alpha.'-sialon ceramics: A review. *Chem Mater* 1991, **3**: 242–252.
[4] Ekström T, Nygren M. SiAlON ceramics. *J Am Ceram Soc* 1992, **75**: 259–276.
[5] Chen IW, Rosenflanz A. A tough SiAlON ceramic based on α-Si_3N_4 with a whisker-like microstructure. *Nature* 1997, **389**: 701–704.
[6] Shen ZJ, Zhao Z, Peng H, *et al.* Formation of tough interlocking microstructures in silicon nitride ceramics by dynamic ripening. *Nature* 2002, **417**: 266–269.
[7] Hewett CL, Cheng YB, Muddle BC, *et al.* Phase relationships and related microstructural observations in the Ca–Si–Al–O–N system. *J Am Ceram Soc* 1998, **81**: 1781–1788.
[8] Wood CA, Zhao H, Cheng YB. Microstructural development of calcium alpha-SiAlON ceramics with elongated grains. *J Am Ceram Soc* 1999, **82**: 421–428.
[9] Wang PL, Zhang C, Sun WY, *et al.* Characteristics of Ca-α-sialon—Phase formation, microstructure and mechanical properties. *J Eur Ceram Soc* 1999, **19**: 553–560.
[10] Liu GH, Chen KX, Zhou HP, *et al.* Low-temperature preparation of *in situ* toughened Yb α-SiAlON ceramics by spark plasma sintering (SPS) with addition of combustion synthesized seed crystals. *Mater Sci Eng A* 2005, **402**: 242–249.
[11] Liu GH, Chen KX, Zhou HP, *et al.* Phase transformation and microstructure development of *in situ* toughened Yb α-SiAlON ceramics prepared by two-step hot-pressing. *Mater Chem Phys* 2006, **98**: 159–164.
[12] Guo FZ, Yin ZB, Li XL, *et al.* Spark plasma sintering of α/β-SiAlON ceramic end mill rods: Electro–thermal simulation, microstructure, mechanical properties, and machining performance. *J Adv Ceram* 2023, **12**: 1777–1792.
[13] Hong DB, Yin ZB, Guo FZ, *et al.* Microwave synthesis of duplex α/β-SiAlON ceramic cutting inserts: Modifying *m, n, z* values, synthesis temperature, and excess Y_2O_3 synthesis additive. *J Adv Ceram* 2022, **11**: 589–602.
[14] Kushan SR, Uzun I, Dogan B, *et al.* Experimental and finite element study of the thermal conductivity of α-SiAlON ceramics. *J Am Ceram Soc* 2007, **90**: 3902–3907.
[15] Zhang SJ, Li F, Du SM, *et al.* Rattling effect in $Yb_aCa_bSi_{7.5}Al_{4.5}O_{1.5}N_{14.5}$ α-SiAlON ceramics. *J Am Ceram Soc* 2025, **108**: 20085.
[16] Zhang SJ, Du SM, Zhang J, *et al.* Influence of stabilizing ions and sintering process on the thermal conductivity of α-SiAlON ceramics. *J Am Ceram Soc* 2023, **106**: 17–23.
[17] Yang RW, Xu J, Guo J, *et al.* High wave transmittance and low thermal conductivity Y–α-SiAlON porous ceramics for high-temperature radome applications. *J Adv Ceram* 2023, **12**: 1273–1287.
[18] Xie RJ, Bert Hintzen HT. Optical properties of (oxy)nitride materials: A review. *J Am Ceram Soc* 2013, **96**: 665–687.
[19] Van Krevel JWH, van Rutten JWT, Mandal H, *et al.* Luminescence properties of terbium-, cerium-, or europium-doped α-sialon materials. *J Solid State Chem* 2002, **165**: 19–24.
[20] Duan CJ, Otten WM, Delsing ACA, *et al.* Photoluminescence properties of Eu^{2+}-activated sialon S-phase $BaAlSi_5O_2N_7$. *J Alloys Compd* 2008, **461**: 454–458.
[21] Joshi B, Kshetri YK, Gyawali G, *et al.* Transparent Mg–α/β-Sialon: Eu^{2+} ceramics as a yellow phosphor for pc-WLED. *J Alloys Compd* 2015, **631**: 38–45.
[22] Jones MI, Hyuga H, Hirao K, *et al.* Highly transparent Lu-α-SiAlON. *J Am Ceram Soc* 2004, **87**: 714–716.
[23] Liu Q, He W, Zhong HM, *et al.* Transmittance improvement of Dy–α-SiAlON in infrared range by post hot-isostatic-pressing. *J Eur Ceram Soc* 2012, **32**: 1377–1381.
[24] Shan YC, Wang G, Liu GH, *et al.* Hot-pressing of translucent Y-α-SiAlON ceramics using ultrafine mixed powders prepared by planetary ball mill. *Ceram Int* 2014, **40**: 11743–11749.
[25] Xiong Y, Fu ZY, Wang H, *et al.* Translucent Mg-α-sialon ceramics prepared by spark plasma sintering. *J Am Ceram Soc* 2007, **90**: 1647–1649.
[26] Ye F, Liu CF, Zhou Y, *et al.* Microstructure and properties of self-reinforced α-sialon ceramics doped with Lu_2O_3. *Mater Sci Eng A* 2008, **496**: 143–149.
[27] Zhu JT, Xu J, Lv S, *et al.* Translucent Y-α-SiAlON ceramics with enhanced mechanical properties prepared from sub-micrometre-sized powders. *Ceram Int* 2020, **46**: 28091–28098.
[28] Grigor'ev ON, Khomenko GE, Perepelitsa NI. Structure and properties of a heterophase ceramic based on α-sialon. *Powder Metall Met Ceram* 1996, **34**: 566–572.
[29] Rosenflanz A, Chen IW. Kinetics of phase transformations in SiAlON ceramics: I. *effects of cation size, composition and temperature. J Eur Ceram Soc* 1999, **19**: 2325–2335.
[30] Kim J, Rosenflanz A, Chen IW. Microstructure control of *in-situ*-toughened α-SiAlON ceramics. *J Am Ceram Soc* 2000, **83**: 1819–1821.
[31] Hirai T, Murao T, Brito ME, *et al.* Effect of Sr addition on thermal

conductivity and mechanical properties of Y-. *ALPHA.'-SiAlON. J Ceram Soc Japan* 2002, **110**: 784–788.
[32] Zhang SJ, Zhang J, Li F, *et al.* Thermal conductivity of Ca α-SiAlON ceramics with varying*m*and*n*values. *J Am Ceram Soc* 2023, **106**: 5642–5647.
[33] Zhang SJ, Zhang J, Li F, *et al.* $Yb_{0.5}Ca_{0.75}Si_{7.5}Al_{4.5}O_{1.5}N_{14.5}$ α-SiAlON ceramics: A hard material with low thermal conductivity. *J Eur Ceram Soc* 2024, **44**: 5957–5964.
[34] Riley FL. Silicon nitride and related materials. *J Am Ceram Soc* 2000, **83**: 245–265.
[35] Yoshimura F, Yamane H. Eu^{2+}-doped strontium aluminum silicon nitrides having α-SiAlON and polytypoid structures. *J Am Ceram Soc* 2017, **100**: 4276–4287.
[36] Shioi K, Hirosaki N, Xie RJ, *et al.* Synthesis, crystal structure, and photoluminescence of Sr-α-SiAlON: Eu^{2+}. *J Am Ceram Soc* 2010, **93**: 465–469.
[37] Toby BH, Von Dreele RB. *GSAS-II*: The genesis of a modern open-source all purpose crystallography software package. *J Appl Crystallogr* 2013, **46**: 544–549.
[38] Redington M, O'Reilly K, Hampshire S. On the relationships between composition and cell dimensions in α-sialons. *J Mater Sci Lett* 1991, **10**: 1228–1231.
[39] van Rutten JWT, Hintzen HT, Metselaar R. Phase formation of Ca-α-sialon by reaction sintering. *J Eur Ceram Soc* 1996, **16**: 995–999.
[40] Schmid HK, Mader W. Oxidation states of Mn and Fe in various compound oxide systems. *Micron* 2006, **37**: 426–432.
[41] Graetz J, Ahn CC, Ouyang H, *et al.* White lines and d-band occupancy for the 3d transition-metal oxides and lithium transition-metal oxides. *Phys Rev B* 2004, **69**: 235103.
[42] Hakeem AS, Khan M, Ahmed BA, *et al.* Synthesis and characterization of alkaline earth and rare earth doped sialon Ceramics by spark plasma sintering. *Int J Refract Met Hard Mater* 2021, **97**: 105500.
[43] Gao BC, Abulaiti W, Guan Z, *et al.* Effect of grain growth in bimodal microstructure on cutting performance of self-toughening Dy-α-SiAlON ceramic tool inserts. *Process Appl Ceram* 2023, **17**: 321–332.
[44] Liu CF, Ye F, Liu LM, *et al.* Effect of post heat treatment on microstructure and mechanical properties of Lu-doped α-SiAlONs.-*J Alloys Compd* 2009, **475**: 735–740.
[45] Wang PL, Zhang C, Sun WY, *et al.* Formation behavior of multi-cation α-sialons containing calcium and magnesium. *Mater Lett* 1999, **38**: 178–185.
[46] Yang ZF, Wang H, Min XM, *et al.* Effect of heating rate on microstructure and properties of spark plasma sintered Li-α-sialon. *Ceram Int* 2011, **37**: 2175–2180.
[47] Zhou CR, Yu ZB, Krstic VD. Pressureless sintered self-reinforced Y-α-SiAlON ceramics. *J Eur Ceram Soc* 2007, **27**: 437–443.